© Springer Nature Switzerland AG 2020
Koji Sugioka
Handbook of Laser Micro- and Nano-Engineering
10.1007/978-3-319-69537-2_39-1

Subtractive Laser Processing Using Extended Depth of Field Focusing

SeungYeon Kang[1] and Craig B. Arnold[2]

(1)Department of Mechanical Engineering, University of Connecticut, Storrs, Connecticut, USA

(2)Department of Mechanical and Aerospace Engineering and Princeton Institute for the Science and Technology of Materials, Princeton University, Princeton, NJ, USA

SeungYeon Kang
Email: sk32@princeton.edu
Email: seung_yeon.kang@uconn.edu

Craig B. Arnold (Corresponding author)
Email: cbarnold@princeton.edu

Abstract

The removal of material through ablative processes has been studied extensively since the development of the laser. As applications employing such processes have become increasingly complex, requiring precise control while increasing speed and throughput, more advanced methods of beam delivery have been developed to achieve these goals. One important emerging methodology is the use of high depth of field optical elements to produce a line focus or other higher dimensional intensity patterns. In contrast to traditional beam focusing where the light is concentrated to a single location in xyz space, by using high depth of field focusing, it is possible to efficiently deliver energy through an extended region of space, thus gaining a number of important benefits for subtractive laser processing. This chapter reviews some of the current methods of producing a high depth of field and discusses the implications and benefits of such approaches for marking, cutting, and drilling of opaque and transparent materials.

Keywords Laser ablation - Laser marking - Laser drilling - Bessel beams - TAG lens - High depth of field optics - Adaptive optics

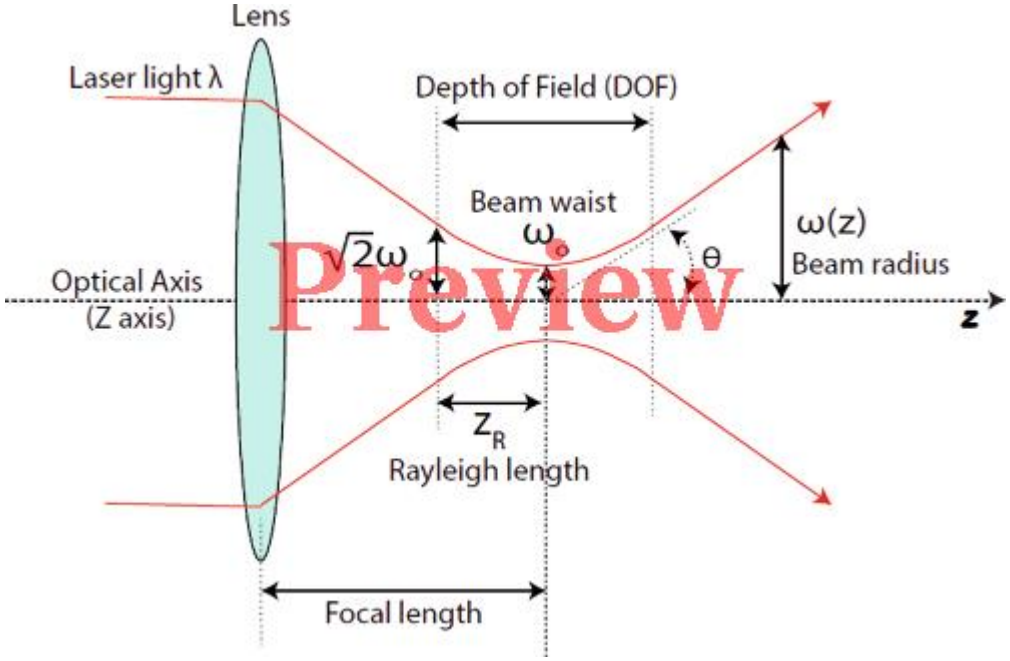
Introduction

Subtractive laser processes, also referred to as laser ablation processes, can include any laser-induced material removal processes, such as cutting, drilling, and surface texturing. In general, the processes take advantage of a sharply focused laser pulse that concentrates the photon energy to a small volume in space, denoted by the focal region. When the surface of a material is co-located

with this focal region and the laser intensity in that location is high, material will be ejected from the surface in a highly energetic ablative process which is discussed in other chapters. Lasers ranging from CW to femtosecond pulsed systems are capable of achieving such conditions, and by optimizing the laser processing parameters, it is possible to achieve a wide variety of commercially relevant structures and material architectures with a great impact on industrial applications across many market spaces.

Over the years, there has been an extensive research on describing the propagation and absorption of laser energy and heat flow during a subtractive laser process, and we will refer the reader to the prior literature on this subject for a more extensive review (Rethfeld et al. *2017*; Nolte et al. *1997*; Brown and Arnold *2010*) [this may be in another chapter]. When dealing with the subtractive processing and ablative removal of material, people typically consider the relevant parameter for the laser to be either laser fluence (energy per unit area) or intensity density (power per unit area), depending on the particular situation. This is based on the premise that the absorption of light occurs within a very small volume at the surface, and so energy and power are normalized by only the area of the interaction. Ablation will occur only above a specific laser fluence or intensity threshold in a given material for a specific wavelength and pulse duration, and thus, this threshold is the main figure of merit reported for a material.

To achieve a sufficient fluence or intensity to overcome the critical threshold for ablation, high numerical aperture (NA) optics are typically used to tightly focus the laser beam into micrometer-sized spots that can produce high-resolution features. From simple geometry ray optics, NA = $n\sin\theta$ where n is the refractive index and θ is the maximum half-angle of the cone of laser beam that enters or exits the optics. The higher the NA, the smaller the laser beam waist (ωo) and the shorter the Rayleigh length ($Z R$) are generated at the focal point. As the beam waist is reduced, the area of the laser interaction decreases, and thus the fluence and intensity increase. This relationship is illustrated in Fig. 1 for a typical collimated Gaussian laser beam.



Preview

If you need to edit the image, please use the original: 453475_0_En_39-1_Fig1_Print.tif

Fig. 1
Description of Rayleigh length, $Z R$, and depth of field (DOF) for Gaussian laser beams

If one considers a Gaussian beam, one can express the fluence as a function of the incident energy E, and the spatial coordinates (r, z) as (Chen et al. *2018*):

$$ {F}_{\mathrm{laser}}\left(E,r,{z}^{\prime}\right)=\frac{2E}{\pi \omega {\left({z}^{\prime}\right)}^2}{e}^{-\frac{2{r}^2}{\omega {\left({z}^{\prime}\right)}^2}}. $$ (1)

where z' is the position along the optical axis relative to the position of the beam waist, $\omega \left({z}^{\prime}\right)={\omega}_o\sqrt{1+{\left(\frac{z^{\prime }}{z_R}\right)}^2}$ is the beam diameter at a particular z' position, ${z}_R=\frac{{\pi \omega}_o^2}{\lambda }$ is the Rayleigh length, and r is the radial coordinate in the x–y plane (Chen et al. *2018*). As we can see from this equation, as the width of the focus is reduced through tighter focusing, the fluence will increase.

The ablation depth, defined as the maximum depth of the ablated surface for a single laser pulse, can be derived from knowledge of the ablation threshold for a given material combined with the laser processing parameters. If we assume the commonly accepted Beer-Lambert model for light absorption in materials, we can directly find the ablation depth, D, as:

$$ D=L\ \ln \left(\frac{F_{\mathrm{laser}}}{F_{th}}\right) $$ (2)

where L is the absorption depth of the laser in the material, F_{laser} is the fluence of the incident laser, and F_{th} is the threshold fluence. By combining Eqs. 1 and 2, we find that for a Gaussian beam, the ablation depth is given by Chen et al. (*2018*):

$$ D\left(E,{z}^{\prime}\right)=L\ln \left(\frac{2E}{\pi \omega {\left({z}^{\prime}\right)}^2{F}_{th}}\right). $$ (3)

And finally we substitute for the beam waist to give us the explicit relation between D and z':

$$ D\left(E,{z}^{\prime}\right)=L\ \ln \left(\frac{2E}{{\pi \omega}_o^2{F}_{th}}\right)-L\ \ln \left(1+{\left(\frac{z^{\prime }}{z_R}\right)}^2\right). $$ (4)

Equation 4 indicates that for standard focused Gaussian illumination on the surface, as one positions the surface further away from the focal point, the ablation depth will decrease accordingly. Now if we consider the absorption depth L for some common materials, for metals as an example, the absorption depth is on the order of 10 nm (Lide *2004*), and for polymers such as polyimide, the absorption depth is in the range of 0.2–0.5 μm under UV illumination (Brannon et al. *1985*). The magnitude of the absorption depth is very small, and, therefore, one can expect that for standard subtractive laser processing, the location of the surface is critical to achieving significant material removal.

Depth of field, often referred to as two times the Rayleigh length (Fig. 1), provides us with less precise, but more straightforward, metric to determine the effective size of the focal region. It is generally understood that when the surface of a material is placed within this focal volume, ablation can occur provided above threshold conditions are achieved. In more practical processing terms, the depth of field gives a tolerance range on how far the surface of interest can be shifted away from the theoretical focal point before losing high resolution.

The tight focusing of a laser beam to achieve high resolution in x-y plane unavoidably produces a shallow depth of field in the axial direction when using traditional spherical optical elements. This result can be seen in Eq. 4 as a smaller z_R will result in the second term of the equation diverging more rapidly as the surface is moved away from the beam waist and the ablation depth more quickly approaching zero.

It is a phenomenon that ultimately hinders laser processing and creates challenges when dealing with surfaces that might be uneven or surfaces where deep hole drilling or machining is necessary. In short, as the location of the surface shifts outside the focal volume, either the material will not be ablated or the resolution of the subtractive process will be substantially reduced.

When dealing with subtractive processes for transparent materials, such as glass or sapphire, the challenges associated with tightly focused beams are similar, albeit the equations above would change. In these cases, if the position of the surface is outside the focal volume, the light could still be focused beneath the surface, and this would preferentially cause material modification at the location of the highest fluence or intensity (Bulgakova et al. *2015*). The result of this additional penetration can further impact the ablative removal of material at the surface and can lead to undesired effects such as surface cracking or reduced resolution (Mirza et al. *2016*). However, under the right conditions, this can be turned into a benefit for high-throughput material removal which will be discussed later in this chapter.

To overcome the challenges associated with matching the location of the surface with the focal volume, industrial manufacturing processes have been developed to manipulate either the focus or the surface to maintain the appropriate positioning. Mechanical positioning of the optics or the surface can be accomplished with traditional motion control stages and robotics. However, these processes come with the cost of added complexity in the system, increased computational cost, requirement for skilled technical support, and reduction in process throughput as the surface must be tracked at all times during the processing. Furthermore, for some advanced precision subtractive processing applications, it can be quite difficult to characterize the position of the surface in real time in order to provide real-time feedback and optimal control over the ablation process.

Extending the Depth of Field

Rather than moving a surface or otherwise attempting to mechanically control the relative positioning of the beam waist and the surface, it has been shown that extended depth of field optical approaches can provide significant benefits for subtractive material processing (Duocastella and Arnold *2013*). If we consider the analysis above, we recognize that if it is possible to increase z_R without substantially affecting the beam waist, then we can maintain above-threshold conditions over a much larger defocus distance, z'. More specifically, if the beam waist is independent of z, the second term in Eq. 4 will approach zero, and the ablation depth will be independent of z.

When dealing with opaque materials, the implication of an extended depth of field is that one would in principle be able to ablate a surface regardless of its location along the optical axis. This would be particular beneficial for surfaces that are not flat where different parts of the surface are at different z positions yet uniform processing is required. Such an approach would obviate the need for mechanical translation of the part or the laser focus and greatly simplify the processing system, leading to the greater process reliability, greater efficiency, and lower processing costs.

In the case of transparent materials, the ablation process is more complicated, and with an extended depth of field, the laser can interact through its bulk. Such processing has important implications for material modification, such as welding and other similar processes. However, for subtractive processing, such an approach has the distinct benefit of being more efficient at removing material over relatively large distances.

In practice, it is not possible to achieve an infinitely long depth of field. However, it is possible to extend the depth of field over modest distances using various forms of diffractive and adaptive optical elements. Armed with these new and advanced optical approaches, it is possible to create line focus beams or other more complex illumination strategies which have enabled high depth of field subtractive laser processing for a wide variety of materials. This chapter discusses the various methods of generating an extended depth of field and introduces several studies on extended depth of field subtractive micromachining processes.

On a side note, extended depth of field is useful not just for laser processing but also for optical trapping (Arlt et al. *2001*; Zhang et al. *2011*; Gao et al. *2017*), 3D printing (Yu et al. *2017*), and real-time volumetric imaging (Lu et al. *2017*; Colomb et al. *2010*; Kang et al. *2018*; Zheng et al. *2018*), in a wide range of applications from laboratory to industry scale. For example, in laboratory applications, extended depth of field is used in microscopy techniques for studying calcium dynamics in neurobioloty (Lu et al. *2017*), 3D imaging of cellular structures (Zheng et al. *2018*), or topography imaging of complex samples (Colomb et al. *2010*). In industrial applications, extended depth of field enables real-time 3D imaging of large objects which can help with rapid-prototyping and metrology analysis capabilites (Kang et al. *2018*).

Generating an Extended Depth of Field

Various methods exist to create an extended depth of field. One way is to use low NA optical elements; however as discussed above, such approaches necessarily increase the beam waist and therefore reduce the lateral resolution. A more useful way to create an extended depth of field without losing lateral focus is to generate a quasi-non-diffracting structured beam. In practice, non-diffracting, and therefore less diverging beams, can be created to focus light over distances that exceed the Gaussian Rayleigh range by several orders of magnitude. There exists a whole family of "diffraction-free" beams that have been demonstrated, including Airy, Bessel, Mathieu, and parabolic beams (Simon *2016*; Salo et al. *2000*). In reality, such beams are not truly diffraction-free (hence "quasi-non-diffracting") since practical devices have finite apertures, and thus they exhibit a range over which they propagate without significant diffraction followed by their spreading in the traditional way. In addition to these structured beams, other methods of creating extended depth of field for laser processing include implementing high-speed varifocal elements which can scan a focus at ultrahigh speeds to create an effective line focus over a large tunable range.

Bessel Beams

Bessel beams are propagating light fields with a distribution described by a Bessel function of the first kind. The concept of non-diffracting Bessel beams has been described at least as far back as the 1940s, but it wasn't until 1975 that mathematical notions of the Bessel beam were constructed and experimentally realized by Durnin et al. (*1987*; Simon *2016*). In cylindrical coordinates, the electric field for the zeroth-order Bessel beam is of the form in Eq. 5, where r and φ are transverse and polar coordinates, z is the coordinate in the propagation direction, and k_z and k_r are the longitudinal and radial wave vectors.

$$ E\left(r,\varphi, z\right)={A}_0\exp \left({ik}_zz\right){J}_o\left({k}_r\right). $$ (5)

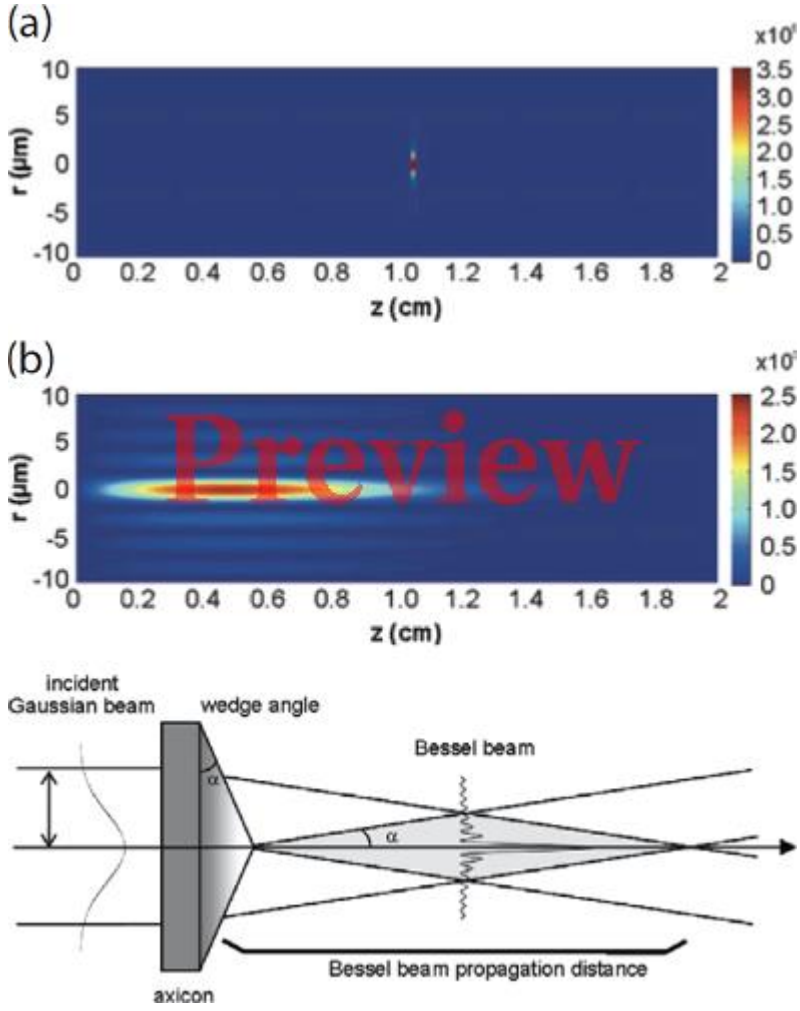
$$ I\left(r,\varphi, z\right)\propto {J}_o^2\left({k}_rr\right). $$ (6)

The beam intensity which can be calculated from Eq. 6 results in a beam cross section of concentric rings. This is often referred to as a non-desirable property of the Bessel beam, leading to unwanted additional ring structures and loss due to energy distribution in the multiple rings.

Another noteworthy property of a Bessel beam is its self-healing or self-reconstruction characteristic. It has been shown with experiments that a Bessel beam can recover its initial intensity profile after being obscured by an obstacle (Fahrbach et al. *2010*). There are several ways to generate Bessel beams, using unique lenses, such as an axicon (McLeod *1954*; Zhai et al. *2009*) or tunable

acoustic gradient lens (Mermillod-Blondin et al. *2008*; McLeod and Arnold *2013*), with an annular aperture placed in the focal plane of a convex lens (Durnin et al. *1987*; Mcgloin and Dholakia *2005*), diffractive optics (Cong and Chen *1998*), or with holograms (Fahrbach et al. *2010*; Turunen et al. *1988*).

An axicon is a conical lens that can be used to generate a Bessel beam (McLeod *1954*; Zhai et al. *2009*). Often considered as the most convenient and cost-effective method, an axicon transforms a laser beam into a Bessel intensity profile, generating an extended depth of field along the optical axis (Simon *2016*). A beam profile difference between a Gaussian beam and an axicon-generated Bessel beam is presented in Fig. 2. As we can see here, a Gaussian beam is focused to a single beam waist that is confined in all three dimensions. In the case of an axicon, the conical surface creates a situation in which light entering the lens at different radii will be focused to different locations along the optical axis. As a result, an axicon creates an interference pattern that resembles a classical "bull's-eye" pattern in the radial plane, while in z-direction, we create a strong line focus over large distances. The length of the line focus region is determined primarily by the cone angle of the axicon, α, combined with the size or aperture of the lens. It is important to note that the intensity figures for the Bessel beam along *rz* plane are reduced by a factor of 7 due to the intensity spread out in the annular rings as compared to the Gaussian case, and as such it is possible to have real-world depth of field expansions of two orders of magnitude while maintaining a similar size in the radial plane.



If you need to edit the image, please use the original: 453475_0_En_39-1_Fig2_Print.tif

Fig. 2

A sketch followed by calculated intensity distributions in axial (*rz*) plane comparing (**a**) Gaussian and (**b**) Bessel beam. Brighter color indicates higher intensity. (**a**) Input Gaussian laser beam is focused to an ellipsoidal focus by converting plane waves into curved wave front. (**b**) An axicon creating a Bessel (Bessel-like) beam. The central lobe forms a line-shaped focus and the Bessel beam consists of conical wave front. (From Duocastella and Arnold (*2012*). Reprinted from Journal of Laser Photonics Rev. 6, No. 5, 607–621 (2012), with the permission of John Wiley and Sons Publishing)

Adaptive optical elements, such as spatial light modulators (SLMs) and deformable mirrors (DMs), are digital devices that modify the phase, amplitude, or polarization of an incoming laser beam and can also be used to create Bessel beams. By producing phase patterns or differentiating arrangements pixel by pixel on SLMs or DMs, one can generate arbitrary beam profiles and holograms for widespread applications in processing and imaging (Sun et al. *2019*; Yao et al. *2018*). In addition to the typical refractive conical axicon lens, SLM holography-generated axicon (Fu et al. *2017*) has also been shown to successfully generate Bessel beams for subtractive laser processing. Such an approach has the benefit of being tunable meaning that one can easily control the parameters of the Bessel beam, such as the length of the non-diffracting region or the number of side lobes in the pattern.

Airy Beams

Just like the Bessel beam, Airy beams are quasi-diffraction-free and self-healing beams, except with a parabolic curve path over a certain distance (Yan et al. *2015*; Hu et al. *2012*). Despite Berry and Balazs' early prediction of Airy function wave packets in 1979 (Berry and Balazs *1979*), the actual experimental demonstration was made rather recently by Siviloglou and co-workers in 2007 (Siviloglou et al. *2007*). Since then, there has been a great interest in the Airy beam and its applications, such as optical trapping (Zhang et al. *2011*), fluorescence imaging (Jia et al. *2014*), light sheet microscopy (Vettenburg et al. *2014*), and laser-induced filamentation (Polynkin et al. *2009*). Airy beams have been realized using diffractive optical approaches including SLMs and DMs (Ma et al. *2018*).

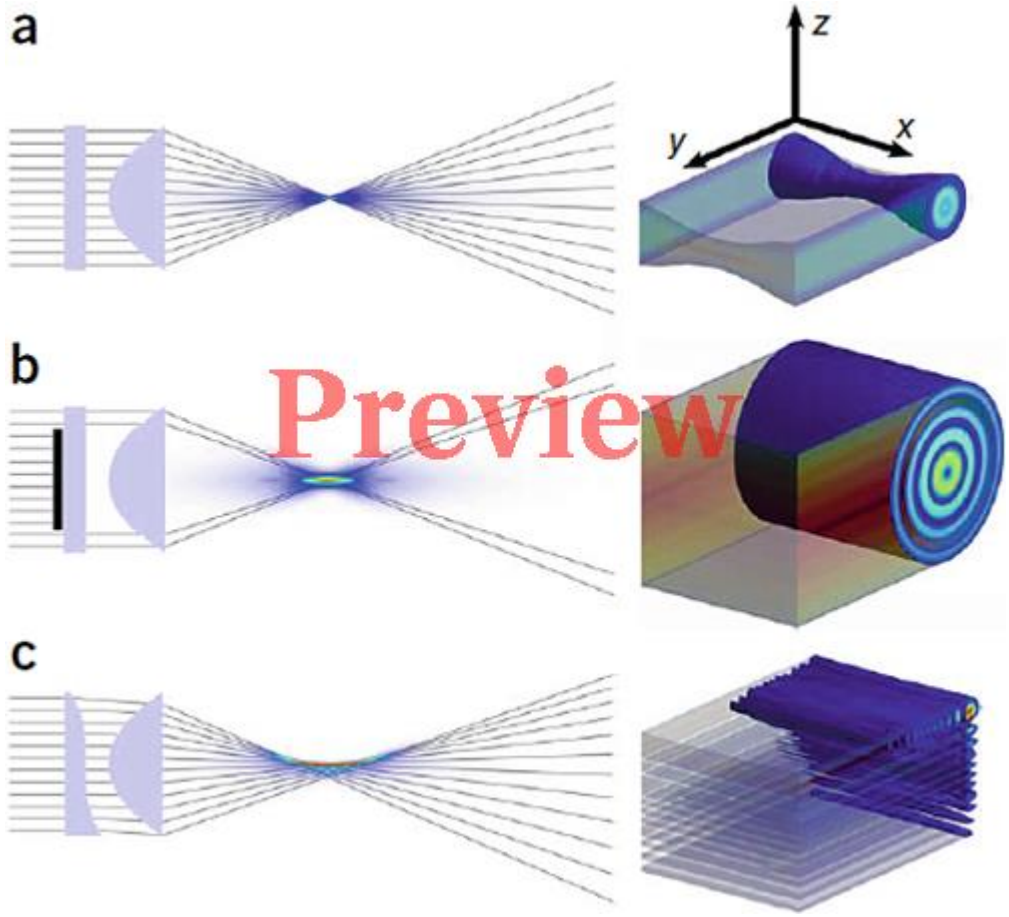
The intensity profile for an Airy beam exhibits the typical Airy wave function in space and can be expressed as Eq. 7 (Zhang et al. *2017*).

$$ \varphi \left(x,z\right)=\mathrm{Ai}\left(x-\frac{z^2}{4}\right)\exp \left[\frac{i}{12}\left(6 xz-{z}^3\right)\right]. $$ (7)

One can see from the term ($x - z^2/4$) that Airy beam follows a parabolic trajectory as it propagates in *z* direction. Although this curvy beam-pathway of Airy beam has often been considered as a non-desirable property, it is recently being explored for micromachining of curvy features (Mathis et al. *2012*) which will be presented as a case study in the later section.

Figure 3 gives an illustration of the beam profile and intensity difference among a Gaussian beam, Bessel beam, and an Airy beam. The left of the figure shows the ray trace paths of three types of beams produced by SLM-generated holograms. Unlike Bessel or Gaussian beams, as the rays propagate in an Airy beam, they are not focused to the center of the optical element, but rather are concentrated at one edge. We see the implications in the intensity profiles on the right side of the image. While the ring structures from the Bessel beam create a more continuous set of light sheets surrounding a bright central core, the Airy beams have discontinuous side lobes in the transverse direction resulting in a set of light sheets that are separated while the peak in intensity or the

diffraction-free region is found along the edge of the pattern. Compared to the Gaussian beam, neither the Bessel nor the Airy beam shows a decrease in the beam waist, verifying the non-diffracting property we expect from these patterns.



Preview

If you need to edit the image, please use the original: 453475_0_En_39-1_Fig3_Print.tif

Fig. 3
Comparison among a Gaussian beam, Bessel beam, and an Airy beam. SLM-generated (**a**) Gaussian, (**b**) Bessel, and (**c**) Airy profile. (From Vettenburg et al. (*2014*). Reprinted by permission from Springer Nature: Nature Methods 11, pages 541–544 (2014), Copyright (2014))

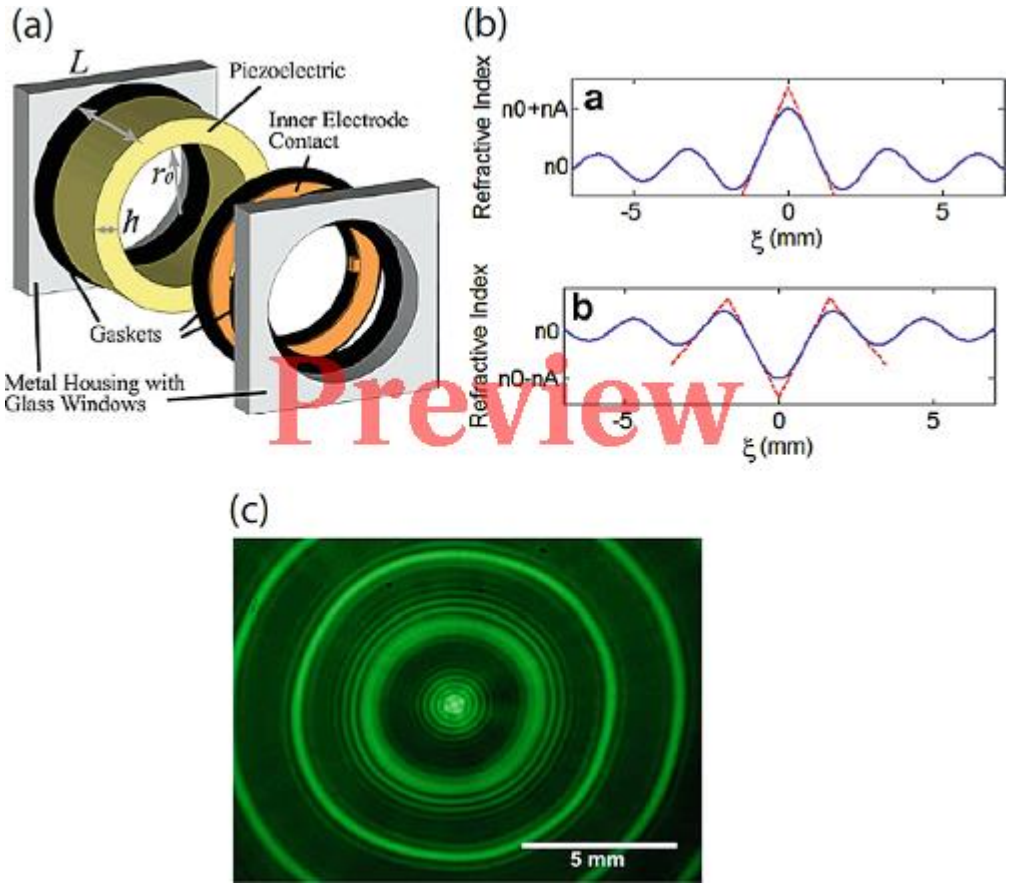
High-Speed Varifocal Optical Elements for Extended Depth of Field

High-speed varifocal optical elements have the ability to rapidly scan the focal position of a beam over very high speeds and thus effectively create a line focus along the optical axis. As long as the unsynchronized z-focus sweep is faster than the total exposure time of the laser, these optical elements can be used to achieve extended depth of field laser processing with a tunable axial range. By implementing high-speed varifocal optical elements, one can eliminate the need for exact surface profiling and readjustment of the focus every time. Therefore, the faster the focus is modulated, the higher the laser processing rate can be achieved.

Various techniques exist to create varying focal optics. Tunable membrane lenses (Oku et al. *2004*), electro-optic ceramic lenses (Kawamura et al. *2015*), and liquid crystal lenses (Lin et al. *2017*) have been shown to modulate the focus. However, the high speed is the key to achieving extended depth of field for subtractive materials processing.

A tunable acoustic gradient (TAG) lens is an ultrahigh-speed varifocal lens that provides an alternative method of creating a tunable extended depth of field. TAG lens, also referred to as an ultrasound lens, is composed of a piezoelectric cylindrical chamber filled with a refractive fluid driven by acoustic waves to modulate the wave front of an incident light beam (Fig. 4a) (Mermillod-Blondin et al. *2008*; McLeod and Arnold *2013*). At a certain resonant frequency, the acoustic wave interferences induced by a driving voltage become constructive, creating a steady-state standing wave (McLeod and Arnold *2013*).

$$ n\left(\rho, t\right)={n}_o+{n}_A{J}_o\left(\frac{\omega \rho}{c_s}\right)\cos \left(\omega t\right). $$ (8)



Preview

If you need to edit the image, please use the original: 453475_0_En_39-1_Fig4_Print.tif

Fig. 4

Schematic and operation of a TAG lens. (**a**) Expanded view of a TAG lens. (**b**) Predicted refractive index profiles at one instant in time (top) with a linear approximation to the central peak profile (red dashed line) and at one half-period later in time (bottom). The scale of the spatial axis is set by the driving frequency. (**c**) Characteristic pattern created by illuminating a circular TAG lens with a wide Gaussian collimated laser beam. Image observed at 80 cm distance after the lens, with driving frequency 299.7 kHz. (From McLeod and Arnold (*2013*). Reprinted from Journal of Applied Physics 102, 033104 (2007), with the permission of AIP Publishing)

The resulting refractive index modulation is as shown in Eq. 8, where n_o is the static index of refraction of the fluid, ω is the driving frequency of the lens, c_s is the speed of sound of the fluid, and ρ is the radial coordinate in the lens plane. n_A is the driving amplitude which is linearly related to the driving power input into the piezoelectric element (McLeod and Arnold *2013*). If one plots this refractive index profile at two instantaneous times separated by half a period, it will be represented as the profiles in Fig. 4b. The incoming beam passing through the liquid refracts based on the refractive index profile in Eq. 3 and forms interference patterns as shown in Fig. 4c, creating a central peak with surrounding ring structures arising from the Bessel function J_o. Therefore, one can picture a TAG lens acting similar to an axicon with a tunable cone angle by adjusting the values of n_A. The rapid scanning with the acoustic driving frequency allows a rapid continuous change in the refractive index. This generates a continuous line focus composed of continuous line of central peak intensities, enabling TAG lens to provide the extended depth of focus.
It is important to note that the line focus created by a scanning lens is characteristically different from the line focus that one obtains through a Bessel or Airy function. In the case of the quasi-non-diffracting beams, the focus is truly stretched out in the propagation direction, and the cost to do that is that energy has to be put into the side lobes. In the case of the TAG scanning lens, at any moment in time, the beam behaves like a traditional Gaussian, but when one averages the intensity over time, we create an effective line focus. The benefit is that the system does not have to lose energy to outer lobes in a pattern and so one is able to more efficiently deliver energy to a surface to be ablated. This has the potential to substantially increase ablation rate and minimize loss throughout a processing system.

Case Studies

Subtractive laser processes include any laser-induced material removal processes, such as cutting, drilling, and surface texturing. Compared to typical chemical or mechanical methods, laser subtractive processing provides direct laser written designs with high temporal and spatial resolutions and minimal material loss. It is also capable of inducing very high heating/cooling rates, thermal gradients, and resolidification rates resulting in higher-quality structuers (Hsu et al. *2011*). Extended depth of field laser processing enabled by the methods described previously can increase the material removal rate without loss in resolution. In this section, we present various case studies on higher-efficiency laser subtractive laser processes achieved by increasing the DOF.

Extended Depth of Field for Surface Structuring

The capability to design and modify surface properties is invaluable in every material processing application since it determines adhesiveness, hydrophilicity, optical and mechanical properties, and tribological properties of the material's surfaces (Kunz et al. *2018*). Moreover, the fabrication of complex surface structures has been used for a wide range of applications, such as bio-sensors (Yang et al. *2014*), cell growth adhesion and isolation (Ta et al. *2016*; Dong et al. *2010*), and photodetectors (Huang et al. *2006*; Gan and Tang *2011*).
To increase the efficiency in laser surface structuring processes, one can use extended depth of field methods to circumvent the necessity to real-time monitor and readjust the focus when machining or marking uneven surfaces. Duocastella et al. used a stack of silicon wafers misaligned with one another to demonstrate extended depth of field surface structuring using a TAG lens. Figure 5a shows a CCD recorded average laser beam intensity map of a typical refractive lens and a TAG lens.

Comparing the beam propagation length, when a TAG lens is inserted into the system, the scanning range is extended by at least three times than that of a normal refractive lens. In Fig. 5b, two lines were direct laser written on a stack of four silicon wafers. In both cases, the laser beam is translated in a line along the edges of the four wafers, representing a non-flat surface. In the case of no focal scanning, the marking only occurs on a single step that has been appropriately positioned in z-direction with respect to the focal position. However, when the extended depth of field is used, marking occurs on all of the steps (ranging over 2 mm in height) without changing the size of the features created. Such processing can be extended to other kinds of surfaces and materials, including transparent materials, and those that undergo multiple laser marking passes.

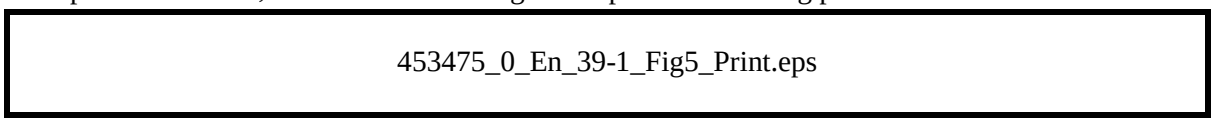
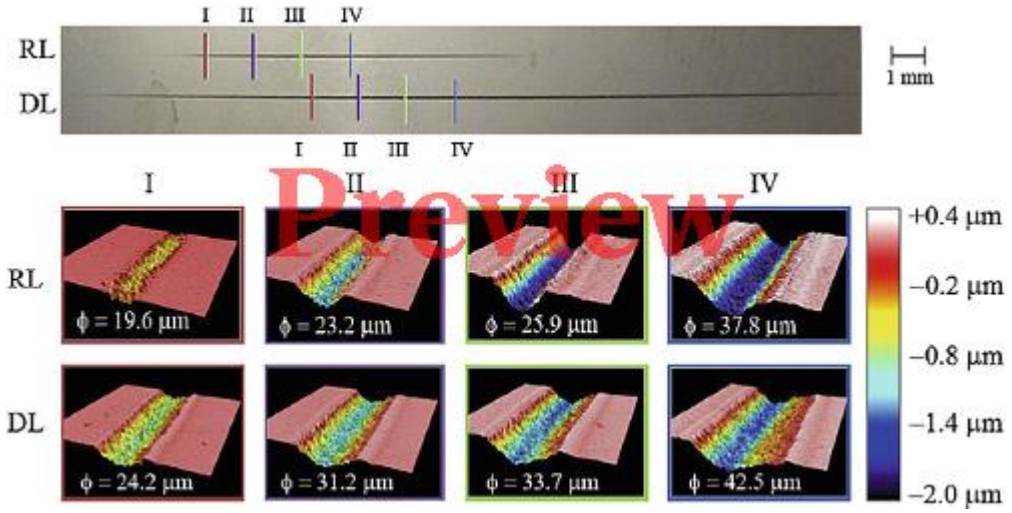


Fig. 5
Laser beam propagation with TAG lens on versus off. (**a**) CCD camera recorded averaged intensity of multiple laser firing events at different distances after the objective. Top: Laser beam propagation after a 5X microscope objective with TAG lens off versus on. Bottom: Corresponding intensity profiles along the axial direction in the beam center. (**b**) Laser machining silicon on stepped surface with 500 μm steps. With TAG lens on, DOF was extended to write lines in each of the four silicon surfaces accounting for a total scanning of 2 mm. The inset scanning electron microscope (SEM) image shows no significant difference between the lines written with the TAG lens on and off. (From Duocastella and Arnold (*2013*). Reprinted from Appl. Phys. Lett. 102, 061113 (2013), with the permission of AIP Publishing)

For ultrafast laser applications, diffractive lenses that increase the depth of field have been shown to increase the micromachining efficiency in surface structuring applications. Due to the large spectral bandwidth for femtosecond lasers, large difference appears in the ablation region when using a diffractive element wherein the focal length is elongated along the propagation direction of the pulse (Torres-Peiró et al. *2014*). To visualize the effect of an increased depth of field, Torres-Peiró et al. direct laser wrote two micro-channels on a tilted stainless-steel sheet. One micro-channel was written with a regular refractive lens and the other was written with a diffractive lens. In this experiment, the tilt is such that as the beam moves across the surface, the surface gradually moves away from the focus location (Fig. 6). No ablation takes place initially due to the far distance from the focus. However, as the beam moves across, it was shown that the channel written with the diffractive lens is over twice in length than the one written with a regular lens. Similar to the TAG scanning experiment, such experiment demonstrates the power of extended depth of field for surface structuring for non-planar surfaces.



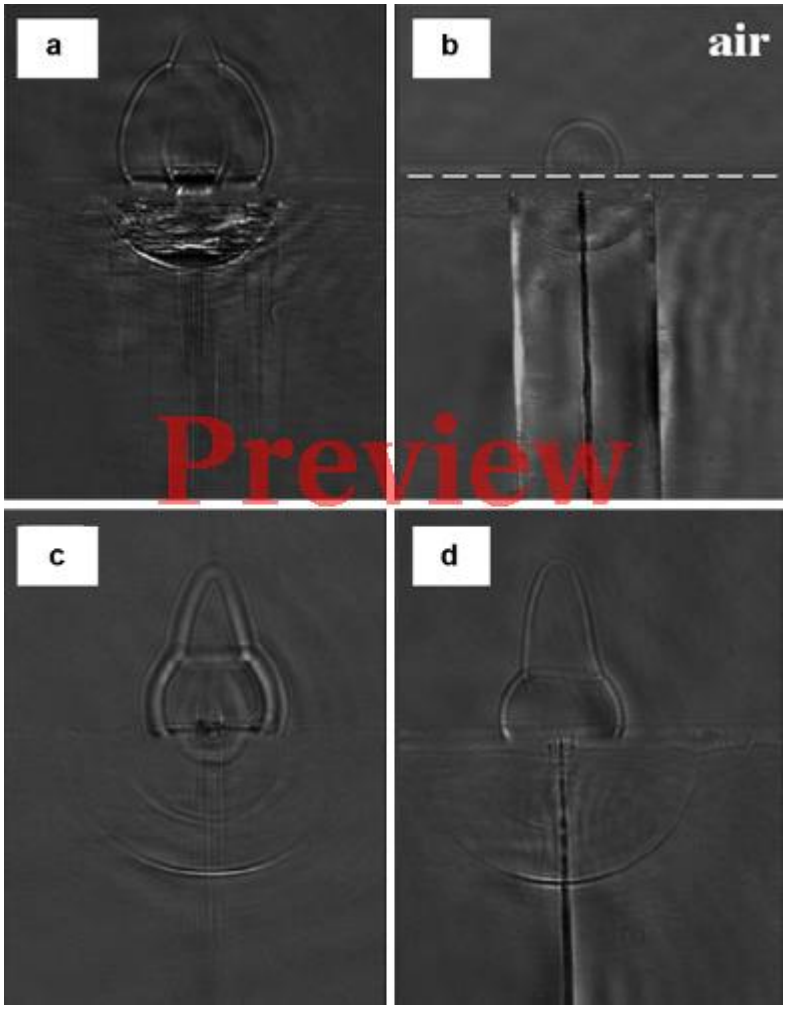
Preview

If you need to edit the image, please use the original: 453475_0_En_39-1_Fig6_Print.tif

Fig. 6
View of the surface of the ablated channels (top). (RL, conventional refractive lens; DL, diffractive lens). The stainless steel sample sheet was tilted at a 21° angle and was translated 20 mm in the tilt direction at a speed of 0.24 mm/s. Confocal microscope images of the different channel regions (bottom). (From Torres-Peiró et al. (*2014*). Reprinted from Applied Surface Science 303, 393–398, Copyright (2014), with permission from Elsevier)

High Aspect Ratio Micro-/Nano-Hole Drilling

High-quality and high aspect ratio microholes are of great research interest in broad applications, such as aeronautical devices (Stephen et al. *2014*), microfluidic devices (Sugioka and Cheng *2013*), and biomedical devices (Miller et al. *2009*). For these applications where deep machining is required, the non-diffracting behavior of a Bessel beams gives an extended depth of field, increasing the tolerance of the focal plane position during material processing and obviating the need of sample translation along the beam propagation direction over multiple pulses. Bessel beam micro-/nano-hole drilling has been demonstrated for various types of materials, including diamond (Kumar et al. *2017*), glass (Courvoisier et al. *2009*; Wang et al. *2017*; Bhuyan et al. *2015*), polymer (Yao et al. *2018*; Wang et al. *2017*; Courvoisier et al. *2013*), and silicon (He et al. *2017*).
A clear difference between a Gaussian beam drilled and a Bessel beam drilled hole is shown in Fig. 7. Wang et al. employed a time-resolved pump-probe shadowgraph technique to analyze the fundamental mechanism during a femtosecond laser single-pulse drilling of PMMA and fused silica (Wang et al. *2017*). An axicon was used to produce the Bessel beam. Looking at Fig. 7a, b, we can see that in the case of the Gaussian ablation, there is a strong shock wave that is created and propagates uniformly away from the ablation location. This shock wave also propagates back into the air above the surface. In contrast, the Bessel beam injects a shock wave directly into the material that is more focused in the direction of optical propagation. Figure 7b shows little shock wave reflecting into the air, and instead, the action of the extended depth of field is to create a long, deep, and uniform removal of material into the bulk. By comparing these cases, it was concluded that the generation of cylindrical shockwave from the Bessel beam is the key for a successful microhole drilling. A high aspect ratio (100:1) Bessel beam drilled PMMA microhole was successfully fabricated using a single femtosecond laser pulse.

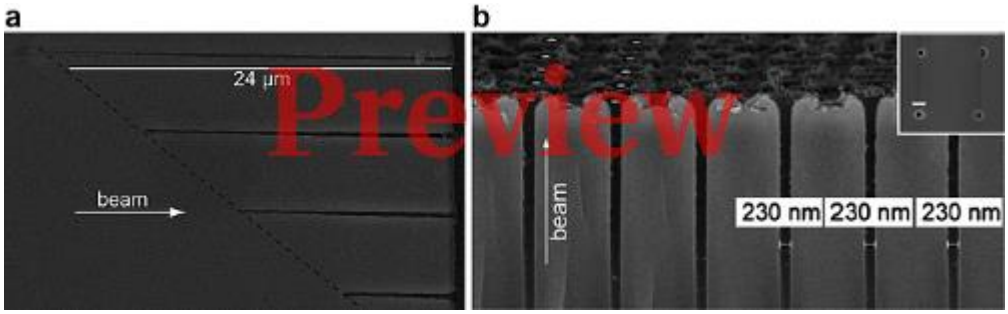


Preview

If you need to edit the image, please use the original: 453475_0_En_39-1_Fig7_Print.tif

Fig. 7
Time-resolved shadowgraph images during single-pulse fs laser Bessel and Gaussian beam drilling of (**a**, **b**) PMMA and (**c**, **d**) fused silica. (**a**) Gaussian beam drilling of PMMA, (**b**) Bessel beam drilling of PMMA, (**c**) Gaussian beam drilling of fused silica, (**d**) Bessel beam drilling of fused silica. All images recorded at a time delay of 30 ns after laser pulse irradiation. The dotted line refers to the boundary of air and sample. (Figure modified from Wang et al. (*2017*). Reprinted from Appl. Phys. Lett. 110, 161907 (2017), with the permission of AIP Publishing)

The benefits of Bessel beam drilling of transparent materials have been further verified by Bhuyan et al. (*2011*, *2015*). Using Corning glass, the team fabricated arrays of Bessel beam drilled nanochannels with a channel length of 10 μm, diameter of 230 nm, and pitch of 1.6 μm (Fig. 8b). Figure 8a shows four various channel lengths that were drilled with the Bessel beam. By varying the Bessel beam onset position by 4 μm for each channel with a motorized translation stage, a high aspect ratio of up to 96:1 was achieved which is significantly greater than what is possible with standard Gaussian optics. Figure 8b demonstrates the high reproducibility that can be achieved. An SEM image from the center of the machined region is shown and the difference in the mean channel diameter was measured to be less than 7%. The minimal achievable distance between the adjacent channels was determined to be 600 nm for the laser parameters used for the experiment (0.70 μJ/pulse) allowing the possibility of a compact array of nanochannels. Residual debris on the surface can be easily removed with post focused ion-beam processing for further industrial use purposes.



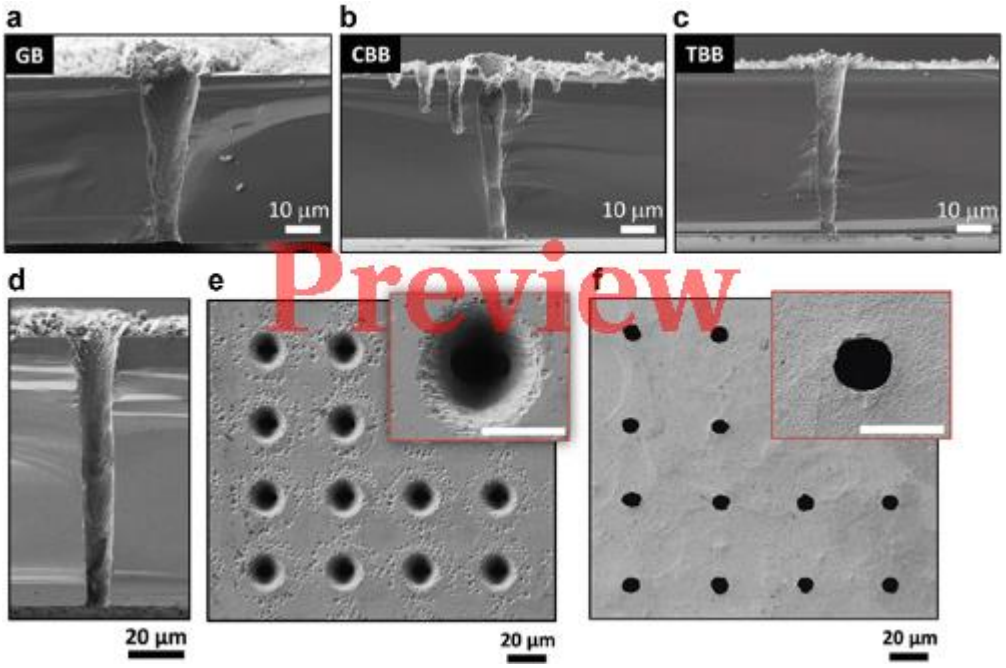
Preview

If you need to edit the image, please use the original: 453475_0_En_39-1_Fig8_Print.tif

Fig. 8

Bessel beam micro-/nano-hole drilling of glass. (**a**) Four varying length channels drilled with the Bessel beam. Diameter is 250 nm, longest channel is 24 μm in length, and the channel length decreases by 4 μm each. (**b**) Profile of an array of Bessel beam drilled channels with channel length 10 μm and diameter of 230 nm. The pitch is 1.6 μm. White circles indicate channel positions. Inset shows postprocessed surface for an additional sample closer to threshold with pitch 800 nm. Scale bar is 200 nm. (From Bhuyan et al. (*2015*). Reprinted from Appl. Phys. Lett. 97, 081102 (2010), with the permission of AIP Publishing)

Figures 9 and 10 present recent progress on tailoring the Bessel beam to improve ablation efficiency for drilling applications. By using SLMs and additional phase masks, it is possible to reduce the side lobes and to further extend the depth of field. He et al. demonstrated the increased efficiency from using tailored Bessel beams by fabricating through-silicon vias (TSVs), which are electrical connections that are crucial during 3D assembly of silicon integrated circuits (He et al. *2017*). The team further shaped an axicon-generated Bessel beam by implementing a specially designed binary phase plate. The tailored Bessel beam (TBB) resulted in a large decrease in the side lobe ratio (i.e., ratio of the maximum peak intensity of the first-order side lobe to that of the central lobe) giving only 0.6%, compared with 15.6% for an axicon-generated conventional Bessel beam (CBB). The higher quality of TSVs fabricated with TBBs can be seen in Fig. 9. Parts a, b and c compare the three different types of beams for ablation, and in the case of a Gaussian, we see the classical tapering of the sidewalls and a large amount of redeposition of material on the surface. A CBB improves the drilling performance, but comes at a cost of high power in the side lobes which structure the surface and create milled regions on their own. The TBB provides the best results with a single, narrow pit in the center with reduced taper and more uniform cross section.



Preview

If you need to edit the image, please use the original: 453475_0_En_39-1_Fig9_Print.tif

Fig. 9

SEM images of through-silicon vias (TSVs) fabricated in (**a**– **c**) 50- and (**d**– **f**) 100-μm-thick Si substrates. (**a**– **c**) are cross-sectional views of TSVs fabricated using a (**a**) Gaussian beam (GB), (**b**) conventional Bessel beam (CBB), and (**c**) tailored Bessel beam (TBB), respectively. (**d**– **f**) are cross-sectional images of the front and rear surface of TSVs produced in 100-μm-thick Si substrates by the tailored Bessel beam, respectively. The scale bars in the insets of (**e**) and (**f**) are 5 μm. (From He et al. (*2017*). Reproduced from Scientific Reports volume 7, 40785 (2017), licensed under the Creative Commons Attribution 4.0 International License)



Preview

If you need to edit the image, please use the original: 453475_0_En_39-1_Fig10_Print.tif

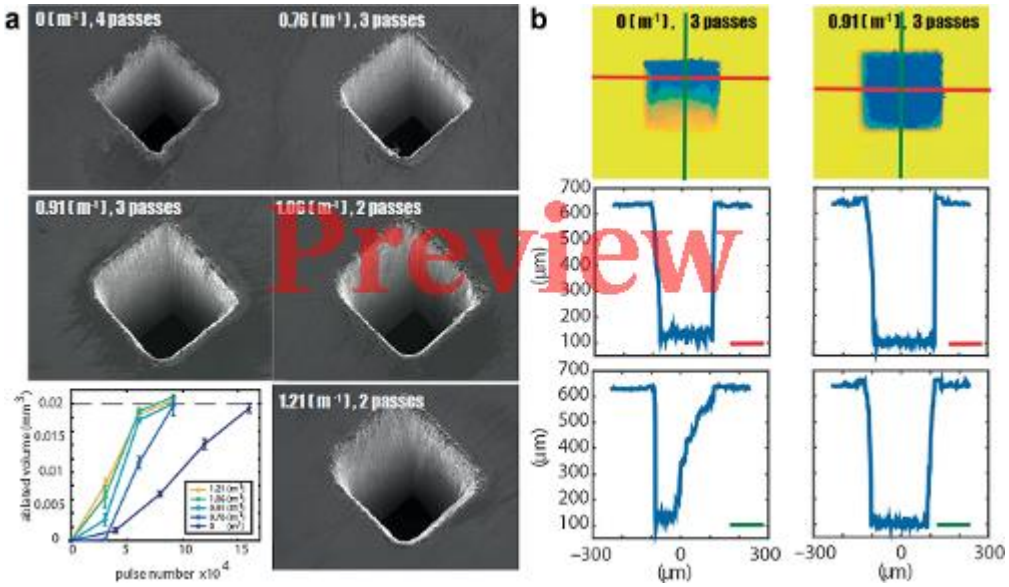
Fig. 10

Drilling results for the three types of beams in PMMA. Compared to regular Bessel beams, Bessel-like beams (BLBs) have the tunability to fabricate both longer and shorter holes. The length scale bar is 100 μm, the diameter scale bar is 2 μm. (From Yao et al. (*2018*). Reprinted from Optics Express 26, 17, 21960–21968 (2018), with the permission of OSA Publishing)

In another case, to add tunability and to extend the depth of field range, Yao et al. used a SLM to generate Bessel-like beams (BLBs). Compared to a regular Bessel beam, BLBs produced by changing the designed phase profile of the SLMs have the ability to control the length of the non-diffracting region similar to changing the cone angle on an axicon. The team was able to achieve BLBs with non-diffraction lengths varying from 10 to 35 mm and was able to demonstrate high-quality, high aspect ratio (560:1) and length-adjustable microholes in PMMA. In Fig. 10, the longer BLBs featured a longer quasi-non-diffraction propagation region along its propagation length, and the shorter BLBs had a more rapid cutoff in the non-diffraction region.

High-Efficiency Micromachining with a TAG Lens

Improvement in micromachining efficiency can be obtained through the ultrahigh scanning speed associated with the TAG lens optical system. Chen et al. demonstrated the increased micromachining efficiency by combining a high repetition rate laser with a TAG lens scanning at over 100 kHz (Chen et al. *2018*). In the experiment, machining of opaque materials was shown to exhibit an increase in material removal rate along with an improvement in sidewall sharpness when irradiated with the extended depth of field scanning method. Figure 11a shows higher-efficiency laser micromachining results of silicon wafers. The team compares five 200-μm by 200-μm, 500-μm depth square ablated silicon holes, each with and without a TAG lens with varying number of laser passes and over different maximum scanning ranges. One pass is accomplished by a bi-directional line scanning over the entire square. While only two passes are required to ablate the square hole with a TAG lens, a total of four passes are required to ablate the same amount of volume without any focus modulation. Figure 11b shows a comparison of horizontal and vertical cross-sectional profiles of two holes, each written without focus modulation and with a TAG lens operation. The square holes micromachined with a TAG lens had clear vertical side walls compared to the ones written without a TAG lens.



Preview

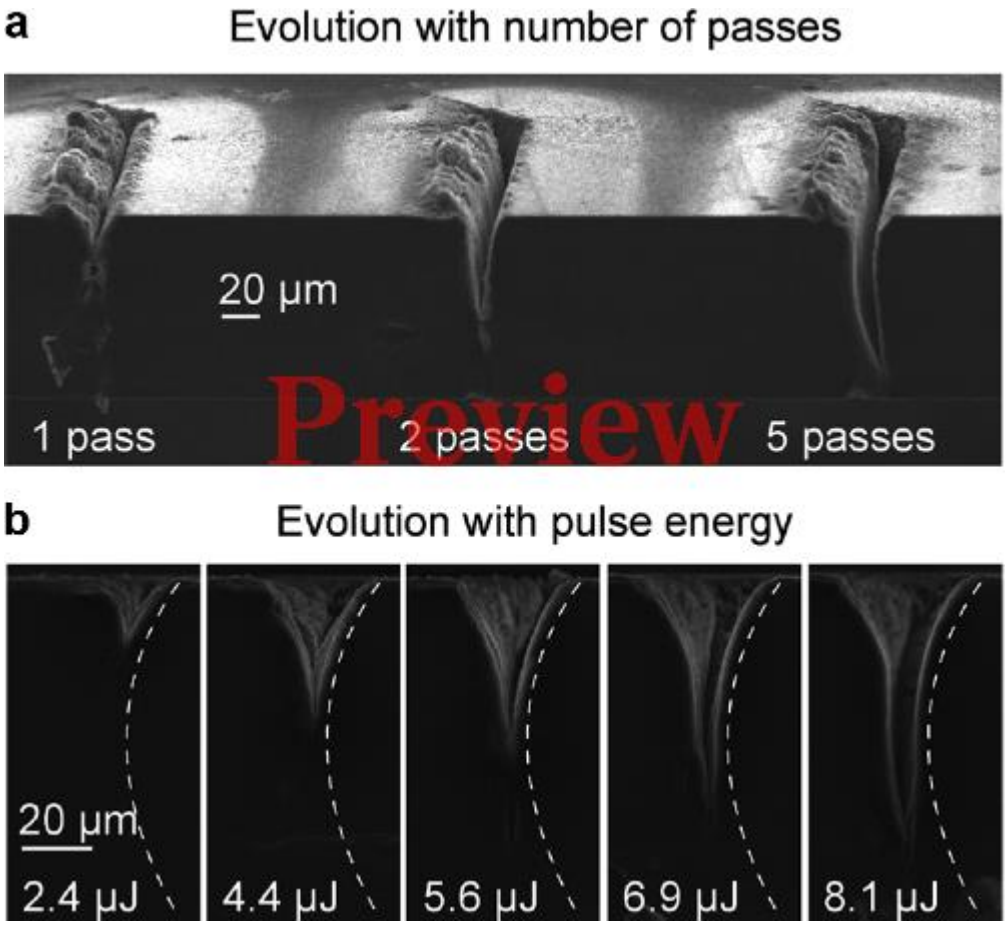
If you need to edit the image, please use the original: 453475_0_En_39-1_Fig11_Print.tif

Fig. 11
(**a**) SEM images of square holes ablated with and without a z-scanner and their measured ablated volume versus pulse number plot. The holes are 200 μm × 200 μm squares with a depth of 500 μm. Without z-scanning (lens power of 0 m), it requires four passes over the substrate to ablate the desired volume. With z-scanning, it requires only three passes with lens powers of 0.76 m and 0.91 m. When the lens power is increased to 1.06 m and 1.21 m, it requires only two passes to reach 90% of the desired ablation volume. (**b**) Horizontal (red) and vertical (green) cross-sectional profiles of holes written with 0 m (no z-scanning) and 0.91 m (z-scanning). The scale bar is 100 μm. (From Chen et al. (2018). Reproduced from Light: Science & Applications volume 7, page 17181 (2018), licensed under the Creative Commons Attribution 4.0 International License)

Micromachining efficiency (i.e., the material removal rate) is heavily dependent on the relative positions of the focal point relative to the substrate surface. As discussed in the introduction and with Eqs. 1, 2, 3, and 4, for standard focused Gaussian illumination on the surface, as one positions the surface further away from the focal point, the laser fluence decreases, resulting in a decrease in the ablation depth. Since TAG lens enables rapid scanning of the focal positions, it eliminates the need for readjusting z-position of the surface. By combining a TAG lens with a rapid firing of the laser, the team was able to guarantee a maximum material removal rate and demonstrate the increased micromachining efficiency. The increased micromachining rate demonstrated in these results suggests possibilities of realizing higher-throughput micromachining for future industrial applications.

Curved-Profile Ablation

The curvy beam pathway of Airy beam has often been considered as a non-desirable property for laser micromachining and drilling due to lack of control over the beam pathway. However, for cases where a simultaneous control of beam steering and sample rotation and translation is required, Airy beams can provide an alternative method for subtractive micromachining of curved trenches with longitudinally varying characteristics both at the surface and within the sample. To demonstrate this result, Mathis et al. successfully micromachined both curved surface profiles and micro-trenches on diamond and silicon samples (Mathis et al. *2012*). A SLM-generated Airy beam was used to direct laser write curved trenches up to 80 μm in depth (Fig. 12). A femtosecond laser was used to minimize the thermally affected zone associated with the ablation process and to guarantee that the thermally affected zone is smaller than the curvature of the target trajectory. These results further extend the state-of-the-art laser material processing technology into a regime where curved features can be generated from just the intrinsic properties of the Airy beam itself rather than from conventional geometric rotational movement of a sample.



Preview

If you need to edit the image, please use the original: 453475_0_En_39-1_Fig12_Print.tif

Fig. 12
Machining of curved trenches in silicon using accelerating beams. (**a**) Variation in trench properties shown for different numbers of passes at a fixed energy of 11 µJ, (**b**) study on the variation in the trench properties a fixed number of 5 passes. (From Mathis et al. (*2012*). Reprinted from Appl. Phys. Lett. 101, 071110 (2012), with the permission of AIP Publishing)

Conclusions

Subtractive laser processing is a versatile method that allows precise removal of a wide range of materials at a controlled rate. Combining extended depth of field optics in the process enables more efficient material removal while obviating the need for real-time monitoring and the inconvenience of readjusting the focus or position of a surface. This chapter discusses the methods and applications of extended depth of field subtractive laser processes. Quasi-non-diffracting beams, such as Bessel and Airy beams, are presented with technologies to generate the beams. While generation of the non-diffractive beams with high quality and high efficiency still remains a challenging issue, there is a large interest in generating higher-quality and tunable extended depth of field beams with adaptive optics and by utilizing acoustic waves to create ultrafast focus modulating optics. The chapter ends with recent case studies on these research interests. As more innovative optical methods continue to develop with an ever-broadening range of capabilities, subtractive laser processing will continue to

improve to achieve even higher laser processing efficiencies for novel applications in both scientific and industrial communities.

References

Arlt J, Garces-Chavez V, Sibbett W, Dholakia K (2001) Optical micromanipulation using a Bessel light beam. Opt Commun 197:239–245
ADS

Berry MV, Balazs NL (1979) Nonspreading wave packets. Am J Phys 47:264–267
ADS

Bhuyan MK et al (2011) Femtosecond non-diffracting Bessel beams and controlled nanoscale ablation. In: 2011 XXXth URSI general assembly and scientific symposium, pp 1–3. https://doi.org/10.1109/URSIGASS.2011.6050591

Bhuyan MK et al (2015) High aspect ratio nanochannel machining using single shot femtosecond Bessel beams. Appl Phys Lett 97:081102
ADS

Brannon JH, Lankard JR, Baise AI, Burns F, Kaufman J (1985) Excimer laser etching of polyimide. J Appl Phys 58:2036–2043
ADS

Brown MS, Arnold CB (2010) Fundamentals of laser-material interaction and application to multiscale surface modification (Chapter 4). In: Laser precision microfabrication, vol 135. Springer, Berlin/Heidelberg, pp 91–120

Bulgakova NM, Zhukov VP, Sonina SV, Meshcheryakov YP (2015) Modification of transparent materials with ultrashort laser pulses: what is energetically and mechanically meaningful? J Appl Phys 118:233108
ADS

Chen T, Fardel R, Arnold CB (2018) Ultrafast z-scanning for high-efficiency micro-machining. Light Sci Appl 7:17181

Colomb T et al (2010) Extended depth-of-focus by digital holographic microscopy. Opt Lett 35:1840–1842

ADS

Cong W, Chen N (1998) Generation of nondiffracting beams by diffractive phase elements. J Opt Soc Am A 15:2362–2364
ADS

Courvoisier F et al (2009) Surface nanoprocessing with nondiffracting femtosecond Bessel beams. Opt Lett 34:3163
ADS

Courvoisier F, Zhang J, Bhuyan MK, Jacquot M, Dudley JM (2013) Applications of femtosecond Bessel beams to laser ablation. Appl Phys A Mater Sci Process 112:29–34
ADS

Dong T et al (2010) A smart fully integrated micromachined separator with soft magnetic micro-pillar arrays for cell isolation. J Micromech Microeng 20:115021

Duocastella M, Arnold CB (2012) Bessel and annular beams for materials processing. Laser Photon Rev 6:607–621
ADS

Duocastella M, Arnold CB (2013) Enhanced depth of field laser processing using an ultra-high-speed axial scanner. Appl Phys Lett 102:061113
ADS

Durnin J, Miceli J, Eberly JH (1987) Diffraction-free beams. Phys Rev Lett 58:1499–1501
ADS

Fahrbach FO, Simon P, Rohrbach A (2010) Microscopy with self-reconstructing beams. Nat Photonics 4:780–785
ADS

Fu S, Wang T, Zhang Z, Zhai Y, Gao C (2017) Non-diffractive Bessel-Gauss beams for the detection of rotating object free of obstructions. Opt Express 25:20098
ADS

Gan Z, Tang Q (2011) Characteristics of laser structured-light sensors. In: Visual sensing and its applications. Springer, Berlin/Heidelberg. https://doi.org/10.1007/978-3-642-18287-7_2
CrossRef

Gao D et al (2017) Optical manipulation from the microscale to the nanoscale: fundamentals, advances and prospects. Light Sci Appl 6:e17039

He F et al (2017) Tailoring femtosecond 1.5-μm Bessel beams for manufacturing high-aspect-ratio through-silicon vias. Sci Rep 7:1–9
ADS

Hsu S-T, Wang H, Satoh G, Yao YL (2011) Applications of surface structuring with lasers. ICALEO Congr Proc 1095–1104. https://doi.org/10.2351/1.5062186

Hu Y et al (2012) Self-accelerating Airy beams: generation, control, and applications (Chapter 1). In: Nonlinear photonics and novel optical phenomena. Springer, New York. https://doi.org/10.1007/978-1-4614-3538-9
CrossRef

Huang Z et al (2006) Microstructured silicon photodetector. Appl Phys Lett 89:14–17

Jia S, Vaughan JC, Zhuang X (2014) Isotropic three-dimensional super-resolution imaging with a self-bending point spread function. Nat Photonics 8:302–306
ADS

Kang S, Dotsenko E, Amrhein D, Theriault C, Arnold CB (2018) Ultra-high-speed variable focus optics for novel applications in advanced imaging, Proc. SPIE 10539, Photonic Instrumentation Engineering V, 1053902; https://doi.org/10.1117/12.2294487

Kawamura S, Imai T, Miyazu J, Sakamoto T, Kobayashi J (2015) 2.5-fold increase in lens power of a KTN varifocal lens by employing an octagonal structure. Appl Opt 53:4197–4201
ADS

Kumar S et al (2017) Study of graphitic microstructure formation in diamond bulk by pulsed Bessel beam laser writing. Appl Phys A Mater Sci Process 123:1–7

Kunz C, Müller FA, Gräf S (2018) Multifunctional hierarchical surface structures by femtosecond laser processing. Materials (Basel) 11:19–26

Lide DR (2004) CRC handbook of chemistry and physics, 85th edn. CRC Press, Boca Raton

Lin Y, Wang Y, Reshetnyak V (2017) Liquid crystal lenses with tunable focal length. Liq. Cryst. Rev. 5, 111–143

Lu R et al (2017) Video-rate volumetric functional imaging of the brain at synaptic resolution. Nat Neurosci 20:620–628

Ma J et al (2018) Generation of high-quality tunable Airy beams with an adaptive deformable mirror. Opt Lett 43:3634
ADS

Mathis A et al (2012) Micromachining along a curve: femtosecond laser micromachining of curved profiles in diamond and silicon using accelerating beams. Appl Phys Lett 101:071110
ADS

Mcgloin D, Dholakia K (2005) Bessel beams: diffraction in a new light. Contemp Phys 46:15–28
ADS

McLeod JH (1954) The axicon: a new type of optical element. J Opt Soc Am 44:592
ADS

McLeod E, Arnold CB (2013) Mechanics and refractive power optimization of tunable acoustic gradient lenses Mechanics and refractive power optimization of tunable acoustic. 033104

Mermillod-Blondin A, McLeod E, Arnold CB (2008) Acoustic gradient index of refraction lens. Opt Lett 33:2146–2148
ADS

Miller PR et al (2009) Laser micromachining for biomedical applications. JOM 61:35–40

Mirza I et al (2016) Ultrashort pulse laser ablation of dielectrics: thresholds, mechanisms, role of breakdown. Sci Rep 6:1–11

Nolte S et al (1997) Ablation of metals by ultrashort laser pulses. J Opt Soc Am B 14:2761
ADS

Oku H, Hashimoto K, Ishikawa M (2004) Variable-focus lens with 1-kHz bandwidth. Opt Express 12:2138–2149
ADS

Polynkin P, Kolesik M, Moloney J, Siviloglou G, Christodoulides D (2009) Curved plasma channel generation in air using ultra-intense self-bending Airy beams. Science (80–) 324:229–232
ADS

Rethfeld B, Ivanov DS, Garcia ME, Anisimov SI (2017) Modelling ultrafast laser ablation. Topical review. J Phys D Appl Phys 50:193001
ADS

Salo J, Fagerholm J, Friberg AT, Salomaa MM (2000) Unified description of nondiffracting X and Y waves. Phys Rev E Stat Phys Plasmas Fluids Relat Interdiscip Top 62:4261–4275

Simon DS (2016) Bessel beams, self-healing, and diffraction-free propagation. In: A guided tour of light beams: from lasers to optical knots 5–1 to 5–15 (Morgan & Claypool Publishers, 2016). https://doi.org/10.1088/978-1-6817-4437-7ch5

Siviloglou GA, Broky J, Dogariu A, Christodoulides DN (2007) Observation of accelerating Airy beams. Phys Rev Lett 99:213901
ADS

Stephen A, Schrauf G, Mehrafsun S, Vollertsen F (2014) New production technologies in aerospace industry – 5th machining innovations conference (MIC 2014) high speed laser micro drilling for aerospace applications. Procedia CIRP 24:130–133

Sugioka K, Cheng Y (2013) Femtosecond laser 3D micromachining for microfluidic and optofluidic applications. Springer Science & Business Media, London

Sun C et al (2019) Theoretical research on the novel adaptive optics configuration based on the tubular deformable mirror for the aberration correction of the annular laser beam. Opt Express 27:9215
ADS

Ta VD et al (2016) Laser textured superhydrophobic surfaces and their applications for homogeneous spot deposition. Appl Surf Sci 365:153–159
ADS

Torres-Peiró S, González-Ausejo J, Mendoza-Yero O, Mínguez-Vega G, Lancis J (2014) Femtosecond laser micromachining with extended depth of focus by using diffractive lenses. Appl Surf Sci 303:393–398
ADS

Turunen J, Vasara A, Friberg AT (1988) Holographic generation of diffraction-free beams. Appl Opt 27:3959
ADS

Vettenburg T et al (2014) Light-sheet microscopy using an Airy beam. Nat Methods 11:541–544

Wang G et al (2017) Cylindrical shockwave-induced compression mechanism in femtosecond laser Bessel pulse micro-drilling of PMMA. Appl Phys Lett 110:161907
ADS

Yan S et al (2015) Accelerating nondiffracting beams. Phys Lett A 379:983–987

Yang J et al (2014) Laser hybrid micro/nano-structuring of Si surfaces in air and its applications for SERS detection. Sci Rep 4:1–8

Yao Z et al (2018) Non-diffraction-length, tunable, Bessel-like beams generation by spatially shaping a femtosecond laser beam for high-aspect-ratio micro-hole drilling. Opt Express 26:21960
ADS

Yu X, Zhang M, Lei S (2017) Multiphoton polymerization using femtosecond Bessel beam for layerless three-dimensional printing. J Micro Nano-Manuf 6:010901

Zhai Z, Ding S, Lv Q, Wang X, Zhong Y (2009) Extended depth of field through an axicon. J Mod Opt 56:1304–1308
ADS

Zhang P et al (2011) Trapping and guiding microparticles with morphing autofocusing Airy beams. Opt Lett 36:2883
ADS

Zhang Y, Zhong H, Belić M, Zhang Y (2017) Guided self-accelerating Airy beams – a mini-review. Appl Sci 7:341

Zheng J, Zuo C, Gao P, Nienhaus GU (2018) Dual-mode phase and fluorescence imaging with a confocal laser scanning microscope. Opt Lett 43:5689
ADS